Tunnelling and Underground Space Technology 152 (2024) 105904

Contents lists available at ScienceDirect

Tunnelling and Underground Space Technology incorporating Trenchless Technology Research

journal homepage: www.elsevier.com/locate/tust

Thermal response to background leakages around an actively heated fiber optic sensor for leak detection in water distribution mains: modeling the effect of heating power and time

Andrea D'Aniello *, Luigi Cimorelli, Domenico Pianese

University of Naples Federico II, Department of Civil, Architectural and Environmental Engineering, via Claudio 21, 80125 Napoli, Italy

ARTICLE INFO

Keywords:
Pipe leakage
Active distributed temperature sensing (ADTS)
Optical fibers
Leak detection and location
Structural health monitoring
Unsaturated zone

ABSTRACT

Fiber optic distributed temperature sensing (DTS) has been recently proposed as a promising technology to detect leaks in water infrastructure. However, it requires a suitable temperature difference between leaked water and the subsurface. Coupling active heating with fiber optic DTS could overcome this limitation, but very limited information is available on its application to leak detection in water pipelines. In this regard, this study addresses for the first time the use of active distributed temperature sensing (ADTS) to detect background leakages, ubiquitous and persistent leaks responsible for large losses and practically undetectable with conventional technologies. The 3D transient analysis of the thermal response to background leakages under different heating powers and times shows that there is potential to detect and locate incredibly small leaks (~ L/d) with a detection threshold of 3 °C when actively heating a fiber optic sensor placed at distance from the pipe, in a location suitable for new and existing pipelines as well as for passive sensors. A potential to quantify background leakages also exists, since nonlinear relationships linking temperature alterations to the leak rate were predicted. The analysis further shows that it is crucial to determine for how long the detection threshold is overcome, and that increasing the heating power is not necessarily the answer. Finally, forced convection is the main heat transfer mechanism around the active sensor once reached by leaked water, and it appears that the chance of altering temperature and quality of water flowing within the nearby pipe and surrounding soil/groundwater would be very limited with ADTS.

1. Introduction

Reducing leaks in water supply infrastructure is more urgent now than ever before. Every day, the global non-revenue water is around 346 million cubic meters according to recent estimates (Liemberger and Wyatt, 2019). A tremendous figure that hits hard considering that this water could meet the needs of millions of people worldwide and instead is lost, together with the energy and the chemicals required for its extraction and treatment, thus also producing an increase in greenhouse gases emissions (FAO, 2012; Stokes et al., 2014). Climate projections are alarming, and prolonged periods of drought are expected to become more frequent in the next years (IPCC, 2023). By 2030, the global demand for water is expected to exceed the available supply by 40 %, and half of the world's population will likely have to face water scarcity (McKinsey & Company, 2009; Mazzucato et al., 2023). Agriculture and industries (from food to high-tech) heavily rely on water, and, in a globalized economy, the effects of water scarcity could unpredictably impact areas not yet affected by the water crisis. Therefore, a more sustainable and conscious use of the available water resource is imperative.

Aging, corrosion, displacements and damages induced by external loads (e.g., land movements, traffic, nearby construction sites, tree roots, etc.), poor initial laying and construction are generally among the factors causing pipelines to leak. The lack of maintenance and rehabilitation further exacerbates the problem. Typically, water companies and managing authorities mostly aim to address reported and unreported leakages, namely bursts and high flow rate leaks in the order of m^3/h (Lambert et al., 2015a; Li et al., 2015; Adedeji et al., 2017; Hu et al., 2021), since these can produce detectable feedback in the infrastructure (i.e., flow rate increases, pressure drops, and acoustic anomalies) as well as in its surroundings (e.g., sinkholes, road pavement collapses, and foundation settlements; Waltham et al., 2005). However, there are also

* Corresponding author.
E-mail address: andrea.daniello@unina.it (A. D'Aniello).

https://doi.org/10.1016/j.tust.2024.105904
Received 10 November 2023; Received in revised form 29 May 2024; Accepted 10 June 2024
Available online 24 June 2024

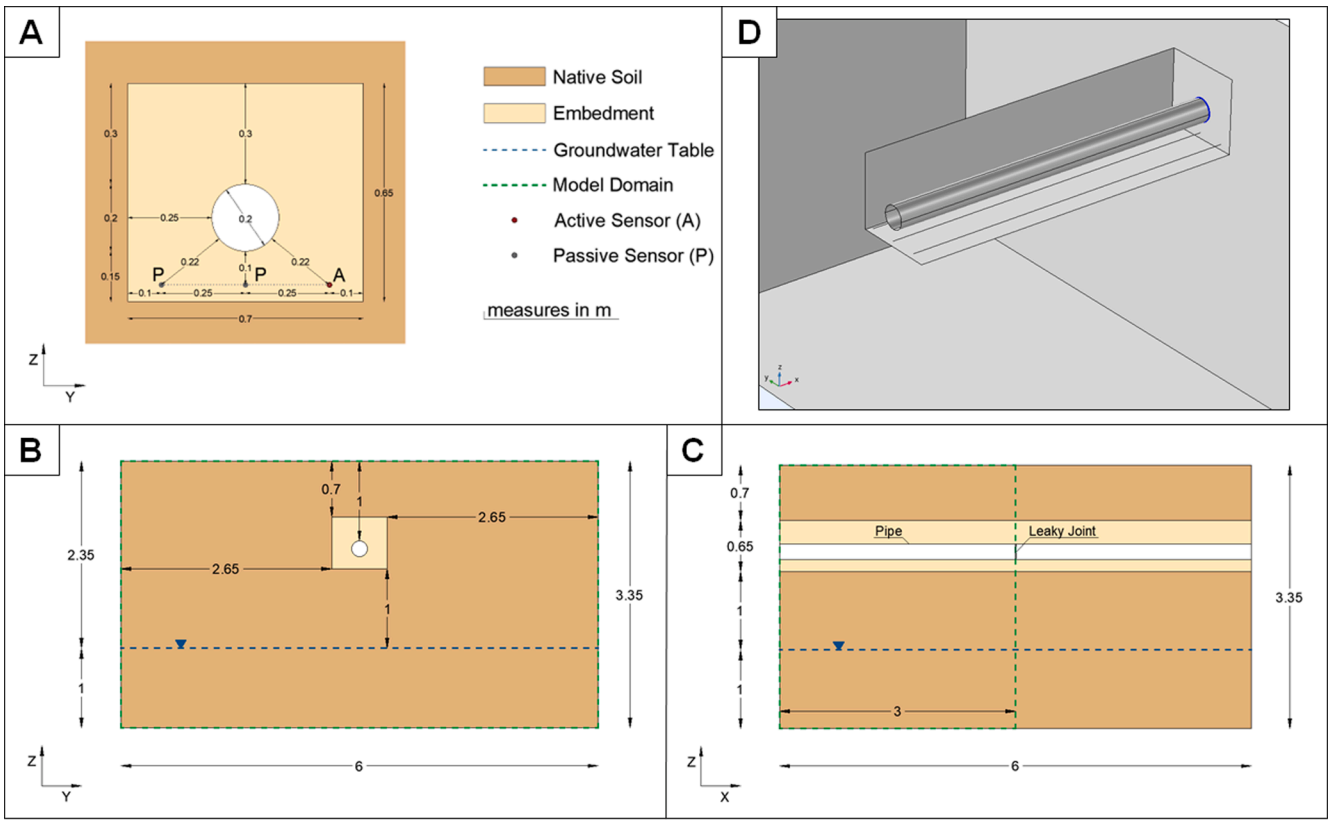

Fig. 1. Detail of the utility trench with leaking pipe, active and passive fiber optic sensors (A), YZ (B) and XZ (C) plane views of the conceptual model, and 3D view of the model domain in COMSOL Multiphysics® (D). Dotted lines in panel (A) are used to better identify the fiber optic sensors.

Table 1
Boundary conditions.

Boundary (geometric entity)	Boundary Conditions	
Top (surface)	no flux fixed temperature [12.5 °C]	
Symmetry plane (surface)	no flux no heat source	
Sides (surface)	fixed hydraulic head [1 m] no heat source	
Bottom (surface)	fixed hydraulic head [1 m] fixed temperature [12.5 °C]	
Pipe outer surface (surface)	no flux fixed temperature [12.5 °C]	
Leaky joint (surface)	flux [5, 25, or 125 L/d], halved due to the symmetry of the model domain fixed temperature [12.5 °C]	
Active sensor (linear segment)	Stationary no flux no heat source	Transient heat source [10, 30, or 60 W/m] for [30, 90, or 180 s]
Passive sensors (linear segment)	no flux no heat source	

Table 2
Soil properties.

Parameter	Embedment	Native Soil
[a]Residual water content [m^3/m^3]	0.045	0.1
[a]Saturated water content [m^3/m^3]	0.43	0.39
[a,*]van Genuchten α parameter [1/m]	14.5	5.9
[a,*]van Genuchten n parameter	2.68	1.48
[a]Intrinsic permeability [m^2]	$9.591 \bullet 10^{-12}$	$4.230 \bullet 10^{-13}$
[b]Solid phase density [kg/m^3]	2000	1900
[b]Solid phase specific heat [J/(kg•K)]	729.9	817.3
[b]Solid phase thermal conductivity [W/(m•K)]	3	2
[c]Longitudinal thermal dispersivity [m]	0.5	0.5
[c]Transverse thermal dispersivity [m]	0.05	0.05

[a] Carsel and Parrish (1988).
[b] The Engineering ToolBox (2001),Dalla Santa et al. (2020).
[c] Diersch (2014).
[*] van Genuchten (1980),Mualem (1976).

other types of leaks that threaten the available water resource: background leakages. From transmission lines to distribution networks, these leaks are ubiquitous and rather insidious, and are responsible for large amounts of water lost despite being individually in the order of L/d (Lambert et al., 1999; Lambert and McKenzie, 2002; Lambert, 2009; Lambert et al., 2015a,2015b). Indeed, background leakages are widespread throughout the infrastructure (generally from defective or damaged joints) and run continuously, going undetected for a very long time, since locally they produce no significant flow rate increase, pressure drop, or acoustic anomaly, despite being highly sensitive to pressure.

However, persistent leaks can produce noticeable temperature alterations in the surrounding soil/utility trench. If collected, this information could help detecting and locating even small leaks, like background leakages. Fiber optic distributed temperature sensing (DTS) could be a viable option for this purpose, since every point of the optical fiber running along the pipeline would act as a sensing element, providing continuous and fast monitoring of temperature (Niklès et al., 2004, Inaudi et al., 2008, and Wijaya et al., 2021). Although optical fibers have been successfully used to monitor strain, temperature, and vibrations for numerous environmental and structural health monitoring problems (Niklès et al., 2004; Inaudi et al., 2008; Bolognini and Hartog, 2013; Wang et al., 2017; Drusová et al., 2021; Wijaya et al., 2021), fiber optic DTS is still being tested for water supply infrastructure (Lombera et al., 2014; Xu et al., 2020; Ibrahim et al., 2021; Wang et al.,

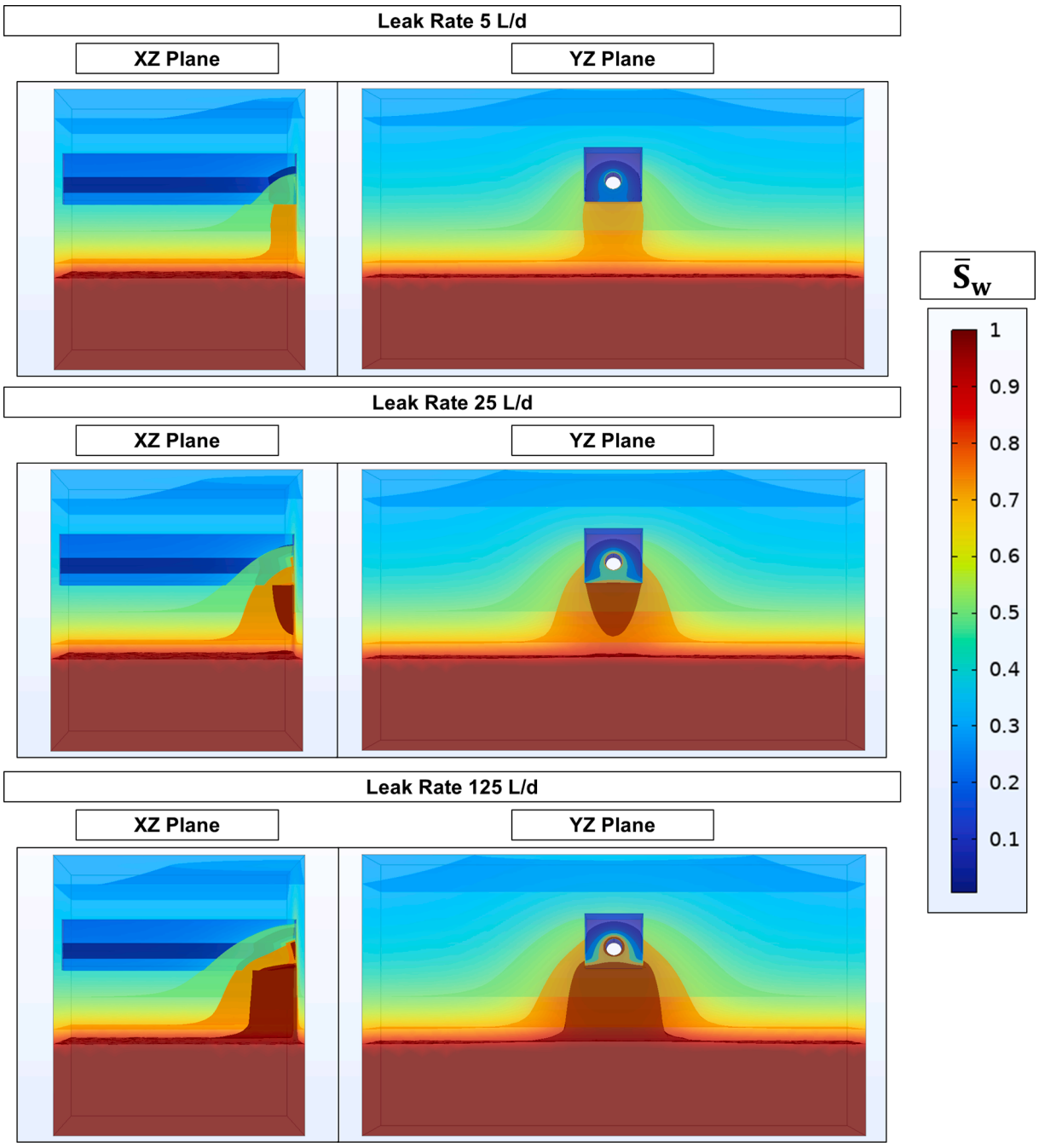

Fig. 2. Predicted final distribution of the effective water saturation ($\bar{S}_w$) for the scenarios with leak rate of 5, 25, and 125 L/d. Transparent colors are used to display the results within the numerical domain.

2022). Indeed, DTS technology offers promising capabilities to detect leaks over tens of kilometers with reasonable spatial and temperature resolutions, and optical fibers are very attractive for pipelines monitoring, being very light and thin, insensitive to humidity, corrosion, and electromagnetic interferences, attachable to practically any surface, long-term durable, and able to work under very harsh conditions (Niklès et al., 2004; Motil et al., 2016; Wijaya et al., 2021). Nevertheless, this technology can be useful only if a sufficient temperature difference exists between water within the pipes and the subsurface. D'Aniello (2023) showed that temperature alterations within the utility trench induced by background leakages with small to moderate temperature differences with the surrounding soil could be potentially detected with fiber optic DTS despite the influence of pipe temperature, although a relatively small detection threshold (0.5 °C) would be required. However, seasonal temperature fluctuations could erase an initially suitable temperature difference between water within the pipes and the surrounding soil for prolonged periods, or this temperature difference could not be suitable at all from the beginning, thus making fiber optic DTS not applicable.

To overcome this limitation, the fiber optic cable could be coupled with a heating cable (an electrical resistance wire) or could be heated itself (using its strength member as electrical resistance) so as to increase the temperature difference with the surrounding soil for a short time, allowing to collect a thermal response that could be linked to leakage. This methodology is known as active distributed temperature sensing (ADTS), which relies on active heating, as opposed to the conventional methodology henceforth referred to as passive distributed temperature sensing (PDTS). Active heating coupled with fiber optic sensing techniques has been used for numerous hydrological and hydrogeological

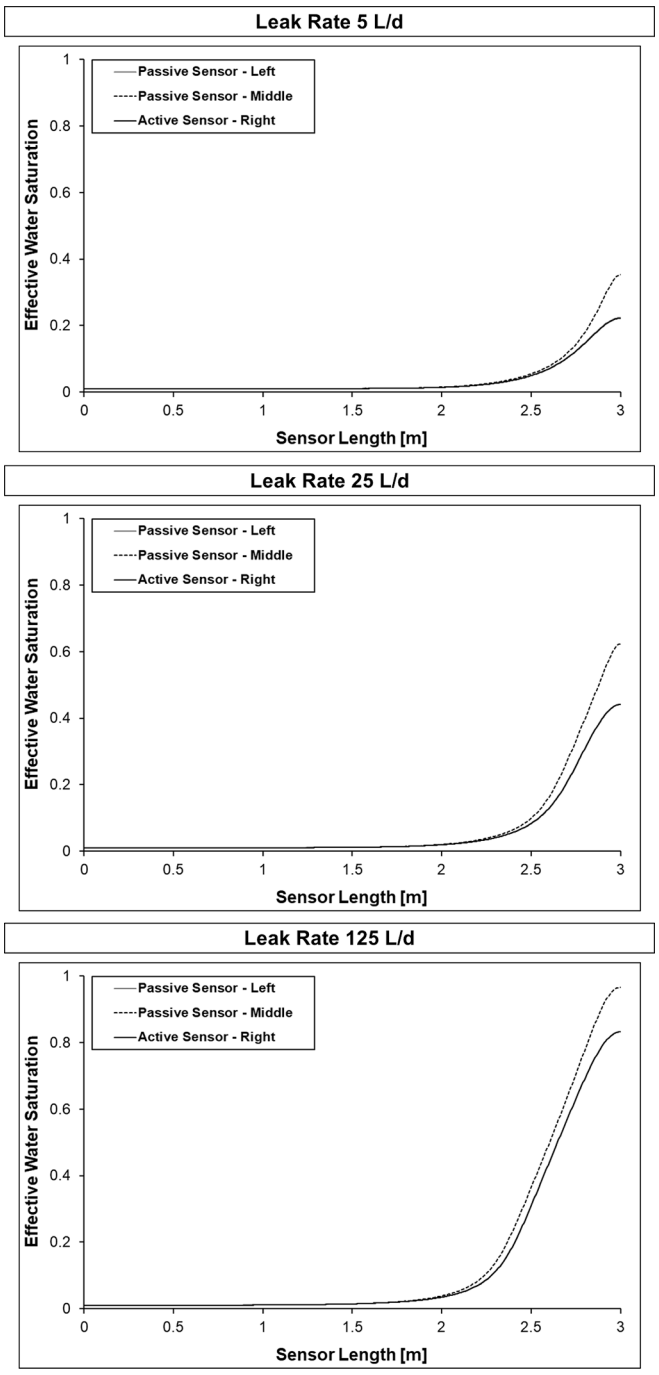

Fig. 3. Predicted final distribution of the effective water saturation along the fiber optic sensors (active and passive) for the scenarios with leak rate of 5, 25, and 125 L/d.

monitoring applications (Su et al., 2017; Vidana Gamage et al., 2018; Sun et al., 2020; del Val et al., 2021; Sun et al., 2022; Liu et al., 2023; Simon et al., 2023; Zhang et al., 2023; Zhu et al., 2023), however, only two studies proposed its application for leak detection in water pipelines, testing it with quasi-distributed (Li et al., 2021) and distributed temperature sensing (Li et al., 2023).

In this framework, the current study aims to add new preliminary theoretical and practical insights to support future field scale experiments and applications of this promising technology, addressing for the first time its application to background leakages. This study offers a detailed transient analysis of the thermal response around an actively heated fiber optic sensor to a wide range of fully developed background leakages in a realistic 3D numerical environment, accounting for the effects of different heating powers and times, of the unsaturated zone, and of fluid properties variation with temperature. To further test ADTS potential to capture incredibly small leaks, as a worst-case scenario there is no initial temperature difference between leaked water and the surrounding soil, and the actively heated fiber optic sensor is placed within the utility trench at distance from the leaking pipe, in a location suitable for both new and existing pipelines, as well as for passive distributed temperature sensing.

2. Methodology

2.1. Conceptual model and outline of the simulations

The conceptual model (Fig. 1) includes a section of a pressurized water distribution main leaking from one of its joints, laid in a utility trench together with two passive fiber optic sensing cables (referred to as passive sensors) and an active one (referred to as active sensor). An unconfined aquifer lies within the native soil with a static groundwater table at 1 m from the bottom of the trench.

Background leakages are set for the entire length of one the joints of the pipeline with leak rates of 5, 25, and 125 L/d, representative of small leaks of long duration that would give practically no pressure, flow, or acoustic feedback in the network. To reproduce a worst-case scenario where passive sensors are ineffective because of the absence of a suitable temperature difference between leaked water and the surrounding subsurface, water flowing within the pipe and the surrounding soil have the same temperature (therefore, the outer surface of the pipe has the same temperature as well and there is no temperature difference), set at 12.5 °C. To maintain a zero temperature difference between leaked water and the surrounding soil (i.e., worst-case scenario), the effects of temperature daily/seasonal fluctuations are neglected.

According to practice (Howard, 1996; Milano, 2012; Yorkshire Water, 2018), the embedment of the utility trench is filled with sand, whereas native soil (a sandy clay loam; USDA SCS, 1987) is chosen for the remaining backfill. Utility trench dimensions (Fig. 1) are chosen to accommodate both rigid and flexible pipes (Howard, 1996; Milano, 2012; Yorkshire Water, 2018).

Following the work of D'Aniello (2023), the three sensing cables (2 passive and 1 active) are placed along the pipe below its bottom (Fig. 1), as with passive sensors these locations showed a better performance compared to others in terms of recorded temperature alterations and detection times of background leakages under different pipe defect configurations, while being suitable for retrofit operations of existing pipelines as well (in particular, those at the sides of the pipe). Furthermore, all cables are placed at sufficient distance from the pipe and the sides of the trench to allow them to potentially work as passive sensors (i.e., so as to reduce the effects of pipe and native soil temperature on the sensing cables if a temperature difference existed). No information on the sensing techniques (e.g., Raman or Brillouin) is given as the conceptual model aims to be as general as possible and does not aim to explore their performance. Type and size of the passive fiber optic cables are not provided since even including all their components (i.e., core, cladding, inner coating, strength member, and outer jacket) their size would fall in a range of few millimeters to roughly a centimeter, thus having practically no influence on the flow behavior of leaked water. The same applies to the active fiber optic cable, as active heating can be provided either by using the strength member as electrical resistance (hence, its size would be the same of a passive sensor) or by adding an electrical resistance wire to the sensing cable, which would increase its size by just a few millimeters. Three heating powers are considered, namely, 10, 30, and 60 W/m, which fall in the range of other relevant ADTS applications (Sun et al., 2022; Li et al., 2023; Simon et al., 2023; Zhang et al., 2023). Heating times are set to 30, 90, and 180 s, in order to be compatible with acquisition times typical of DTS systems used for kilometers long applications (Niklès et al., 2004; Inaudi et al., 2008;

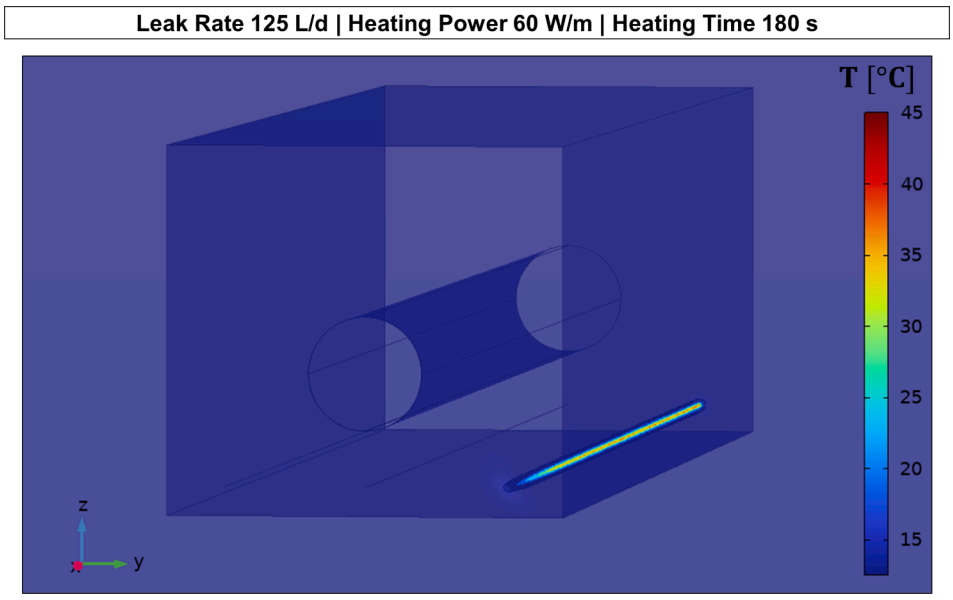

Fig. 4. Predicted temperature (T) distribution at 180 s for the scenario with leak rate of 125 L/d, heating power of 60 W/m, and heating time of 180 s. Only the utility trench and its close surroundings are presented as temperature varies just in proximity to the actively heated fiber optic sensor. Transparent colors are used to display the results within the numerical domain.

Bolognini and Hartog, 2013) and to reduce as much as possible the electrical power supply used for active heating.

Two different time frames are considered for the simulations. At first, simulated leaks are allowed to reach steady state, therefore a stationary solution is achieved for each leak rate modeled, for a total of 3 stationary simulations. Then, active heating is turned on with heating power and time defined as above, and for each scenario transient simulations are performed up to 600 s (10 min) to fully observe the thermal response around the active sensor during heating and cooling. Overall, a total of 27 transient simulations were performed accounting for 3 different leak rates (5, 25, and 125 L/d), 3 heating powers (10, 30, and 60 W/m), and 3 heating times (30, 90, and 180 s).

2.2. Numerical modeling

Version 6.1.0.346 of COMSOL Multiphysics® (COMSOL, 2022) was used to model the different scenarios. In particular, the Richards' Equation interface (Subsurface Flow module) was used to solve the pressure-based formulation of the generalized form of the equation of groundwater flow through variably water saturated porous media (Bear, 1972; Istok, 1989; COMSOL, 2022). This interface was coupled with the Heat Transfer in Porous Media interface (Heat Transfer Module) to solve simultaneously the heat equation under the assumption of local thermal equilibrium (Nield and Bejan, 2013; COMSOL, 2022). Details on the mathematical formulation of the governing equations solved by COMSOL with the finite element method are provided in the Appendix.

The numerical domain takes advantage of the symmetry of the problem with respect to the cross-sectional plane (YZ plane) passing through the leaky joint (modeled as a 0.5 cm long portion of the outer surface of the pipe), and its dimensions (3 m × 6 m × 3.35 m, Fig. 1) are sufficient to avoid any potential interaction of leaked water with the boundaries of the domain. To capture the flow and the heat transfer processes occurring along the sensing cables, the model domain is discretized with a considerably fine mesh consisting of 2′047′668 irregular tetrahedra.

Initial conditions used for the three stationary simulations are a hydraulic head of 1 m (as water within the unsaturated zone is assumed in equilibrium with the static groundwater table prior to the onset of the leaks) and a temperature of 12.5 °C for the whole domain according to the conceptual model described in sec. 2.1. The stationary solution achieved for each leak rate (5, 25, and 125 L/d) provides the initial conditions prior to active heating used for the transient simulations. Boundary conditions are provided in Table 1. Convergence of the nonlinear solver is ensured by a relative tolerance of 0.001, whereas the time step used for transient simulations depends on convergence history with a maximum set to 1 s to have a sufficiently fine temporal discretization during active heating. Each computation was performed on an Intel®Core™ i9-8950HK CPU running at 2.9 GHz with 16 GB RAM and took about 2 h.

The temperature dependence of air and water properties (listed in the Appendix) is reproduced in the numerical model with polynomial interpolations of the data presented in The Engineering ToolBox (2001). Conversely, the pressure dependence of fluid properties is neglected because modeled pressure alterations are insignificant in this regard. Hydraulic and thermal properties of trench filling material and native soil are provided in Table 2.

3. Results

3.1. Leaked water pathway before and during active heating

Leaked water predominantly moves downwards in the native soil supported by gravity, and its spreading within the embedment is limited (Fig. 2). As the leak rate increases, the extent of the plume of leaked water increases, as well as water saturation inside it. To better understand the flow behavior of water leaked from buried pipelines, the interested reader can find more information in D'Aniello et al., (2021,2022). Definitions of water saturation and effective water saturation are provided in the Appendix.

The distribution of leaked water does not change from its steady-state configuration during active heating. Indeed, the plume of leaked water remains symmetric despite active heating occurring on the right side, and the distributions of effective water saturation along the passive sensor on the left and the active sensor on the right are identical regardless of heating power and time (Fig. 3). This occurs because the heating time is rather limited (up to a maximum of 180 s) to result in any significant temperature rise in the surrounding soil other than at the close vicinity of the actively heated sensing cable (the closer to the cable, the higher the temperature). Indeed, at the maximum heating power and time (60 W/m and 180 s), the temperature rise occurs up to just 1–2 cm

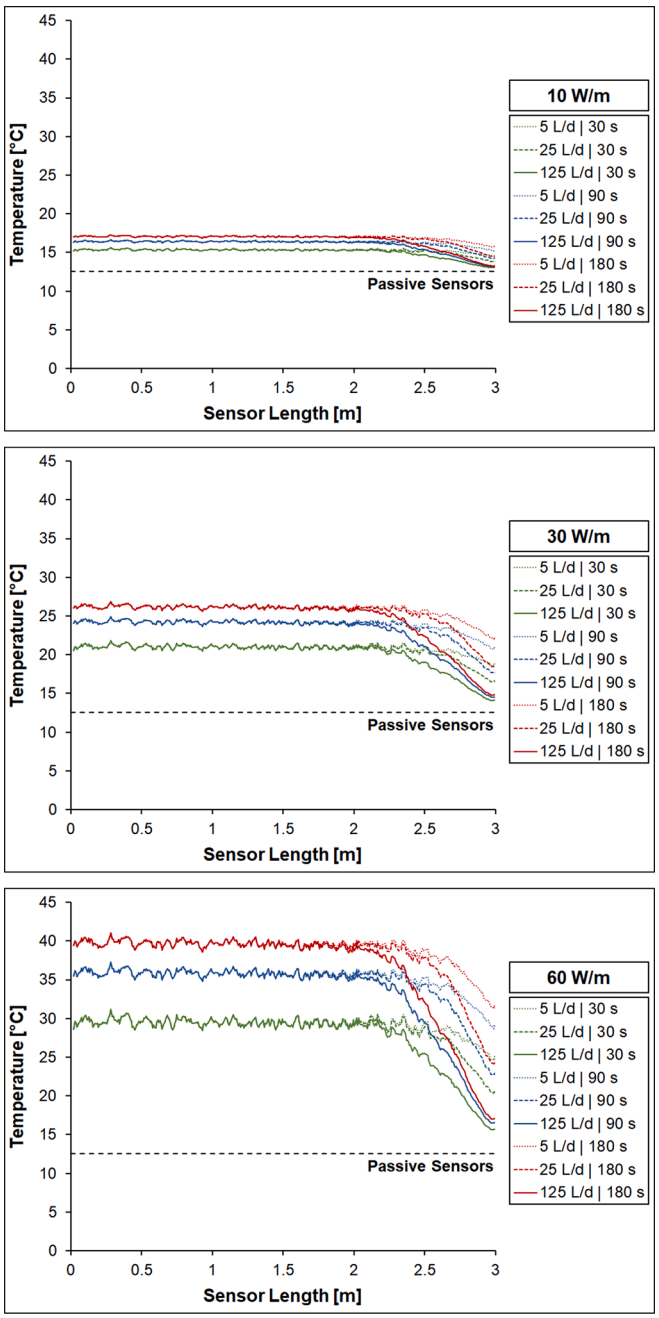

Fig. 5. Predicted temperature distribution along the actively heated fiber optic sensor at the end of the heating phase for each scenario, grouped according to the heating power. The dashed line represents the predicted temperature distribution along the passive sensors.

around the active sensor (Fig. 4), with a maximum temperature at distance from the leak of about 40.6 °C (roughly 28 °C higher than the initial temperature) just at the end of the heating phase. Conversely, when heating power and time are the lowest (10 W/m and 30 s), the maximum temperature rise at distance from the leak is about 15.3 °C at the end of the heating phase (Fig. 5), roughly 3 °C higher than the initial temperature. Therefore, fluid properties variation with temperature is rather limited, occurring for a short time in a very limited space, and it is not sufficient to induce any noticeable natural convection phenomena, and thus any change in the overall flow field.

3.2. Temperature profiles along the sensing cables

As expected, at distance from the leak temperature is practically uniform along the active sensor and increases as heating power and time increase (Fig. 5). Since at these locations there is no appreciable variation in the flow field either due to leaked water migration within the embedment or due to active heating (sec. 3.1.), heat transfer here is conduction dominated (no natural or forced convection occurs). However, a clear temperature drop can be noticed in proximity to the leaky joint, suggesting the presence of a forced convection mechanism.

The length of active sensor affected by the temperature drop depends on the leak rate and increases with it (Fig. 5), as leaked water spreads more within the embedment at higher leak rates (sec. 3.1.). At given heating power and time, the temperature drop becomes more pronounced as the leak rate increases, further indicating the convection-dominated nature of the heat transfer mechanisms occurring along the active sensor in proximity to the leaky joint. In addition, as the leak rate increases and the heating power decreases, temperatures reached along the active sensor at the leaky joint tend to get closer to each other despite the different heating times. Instead, at given leak rate, the temperature drop increases and is more abrupt as heating power and time increase, simply because the heat flux is higher and/or lasts longer, thus allowing the active sensor to reach higher temperatures. Consistently with what shown in sec. 3.1., the two passive sensors experience no temperature alteration along their length, always maintaining the initial soil temperature (12.5 °C).

3.3. Recorded temperatures over time along the actively heated sensing cable

Predicted temperatures recorded over time along the active sensor are presented hereinafter (Figs. 6-8). To reproduce measurements taken over time by a hypothetical DTS system used for kilometers long applications, temperatures along the active sensor are averaged over a length equal to the sampling distance typical for a spatial resolution of 1 m, namely 0.2 m (halved due to the symmetry of the model domain). Specifically, two locations are considered along the active sensor: the leaky joint, denoted as "Leak", and the farthest point from the leak (at a distance of 3 m), denoted as "Far".

During heating, temperature increases in all cases along the active sensor, reaching a maximum at the end of the heating phase. As heating stops, temperature decreases abruptly at the beginning of the cooling phase, and then asymptotically moves towards the temperature prior to active heating. As heating power and time increase, recorded temperatures increase as well over time, whereas their growth rate increases with increasing heating power. Because of the effect of forced convection induced by the leaks, recorded temperatures are always the lowest at the leaky joint and decrease as the leak rate increases, together with their growth rate. These aspects are further evident from Fig. 9, where recorded temperature variations over time with respect to the temperature prior to active heating are plotted on a semi-$\log_{10}$ scale for all scenarios. Fig. 9 also shows how temperatures recorded along the active sensor increase logarithmically over time during active heating, and then decrease in a power law fashion during the cooling phase.

To explore the ability of the active sensor to detect the selected leaks, the difference between the temperatures recorded over time at the farthest point from the leak ("Far") and at the leaky joint ("Leak") is also plotted in Figs. 6-7-8 and compared to a detection threshold. In absence of a conventional threshold used for leak detection in water pipelines with ADTS, this is set to 3 °C, which is generally suggested for PDTS in similar applications (Ziemendorff, 2022). Overall, the behavior of the temperature difference recorded over time between these two opposite locations along the active sensor (i.e., "Far" and "Leak") is pretty similar to the one described previously for the recorded temperatures. In particular, the temperature difference increases with increasing leak rate, heating power and time, becoming more and more pronounced

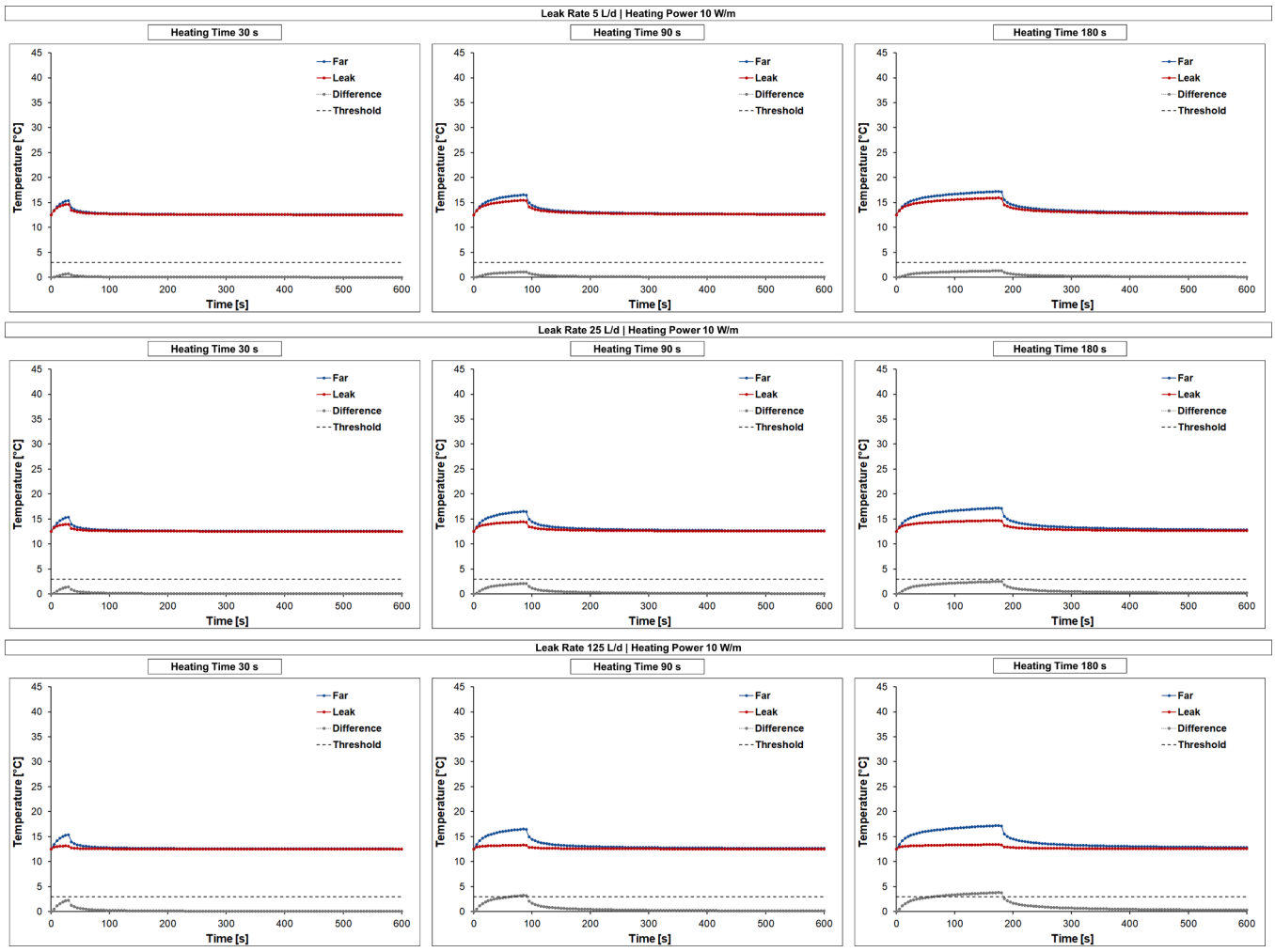

Fig. 6. Predicted temperature recorded over time along the actively heated fiber optic sensor at the farthest point from the leak ("Far") and at the leaky joint ("Leak") together with the difference over time ("Difference") between the predicted temperatures at these locations for all scenarios with heating power of 10 W/m. The dashed line represents the chosen detection threshold of 3 °C.

over time during the heating phase and reaching maximum values at the end of it. Indeed, at 60 W/m the selected detection threshold is overcome in all cases, whereas at 30 W/m the recorded temperature difference fails to overcome this threshold only when leak rate and heating time are the lowest (5 L/d and 30 s). Conversely, at 10 W/m the selected threshold is overcome only when the leak rate is the highest (125 L/d) and at higher heating times (90 and 180 s). The time over which the selected detection threshold is overcome strictly depends on heating time and power and increases with these.

4. Discussion

The predicted thermal response to background leakages around the actively heated fiber optic sensor modeled in this study (sec. 3.) shows that there is potential to detect and locate incredibly small leaks (from 5 to 125 L/d) in buried water pipelines with active distributed temperature sensing. These leaks would remain undetected otherwise since they give no local feedback within the pipeline in terms of flow rate increase, pressure drop, or acoustic anomaly. As a result, the actual health of the water infrastructure would remain unknown, thus hindering a proper planning of maintenance, repair, and rehabilitation operations that could prevent further deterioration of the infrastructure. Furthermore, the knowledge of the actual distribution of background leakages throughout the water infrastructure would also support the formulation of tailored pressure management strategies that would help reducing the large amount of water lost through these small but persistent and ubiquitous leaks.

Indeed, the numerical analysis showed that actively heating a fiber optic sensing cable at 30 W/m and for 90 s could be sufficient to overcome a detection threshold of 3 °C for leaks as small as 5 L/d, which is an extremely small value if compared to the usual targets of leak detection and location operations (generally in the order of m^3/h). A lower heating power could be used as well, depending on the targeted leaks. Indeed, a heating power of 10 W/m for 90 s proved to be sufficient to overcome the same detection threshold for leaks as low as 125 L/d. Conversely, increasing the heating power up to 60 W/m allowed to overcome the detection threshold for the smallest leak modeled (5 L/d) even with the shortest heating time (30 s). However, it is important to recall that the DTS system would require a certain amount of time (i.e., the acquisition time) to retrieve the signal from a given location at a given spatial and temperature resolution. Therefore, it is also crucial to determine for how long the detection threshold is overcome, so as to allow the DTS system to acquire the desired information and give back the alarm. Hence, the highest heating power possible is not necessarily the answer, and a compromise between heating power and time should be found depending on the acquisition time of the DTS system (which strongly depends on the length of the pipeline to monitor, the detection threshold, the required spatial and temperature resolutions), but also on the monitoring strategy (e.g., the numbers of acquisitions during the day, the targeted leak rates, and the detection threshold), on the cost of

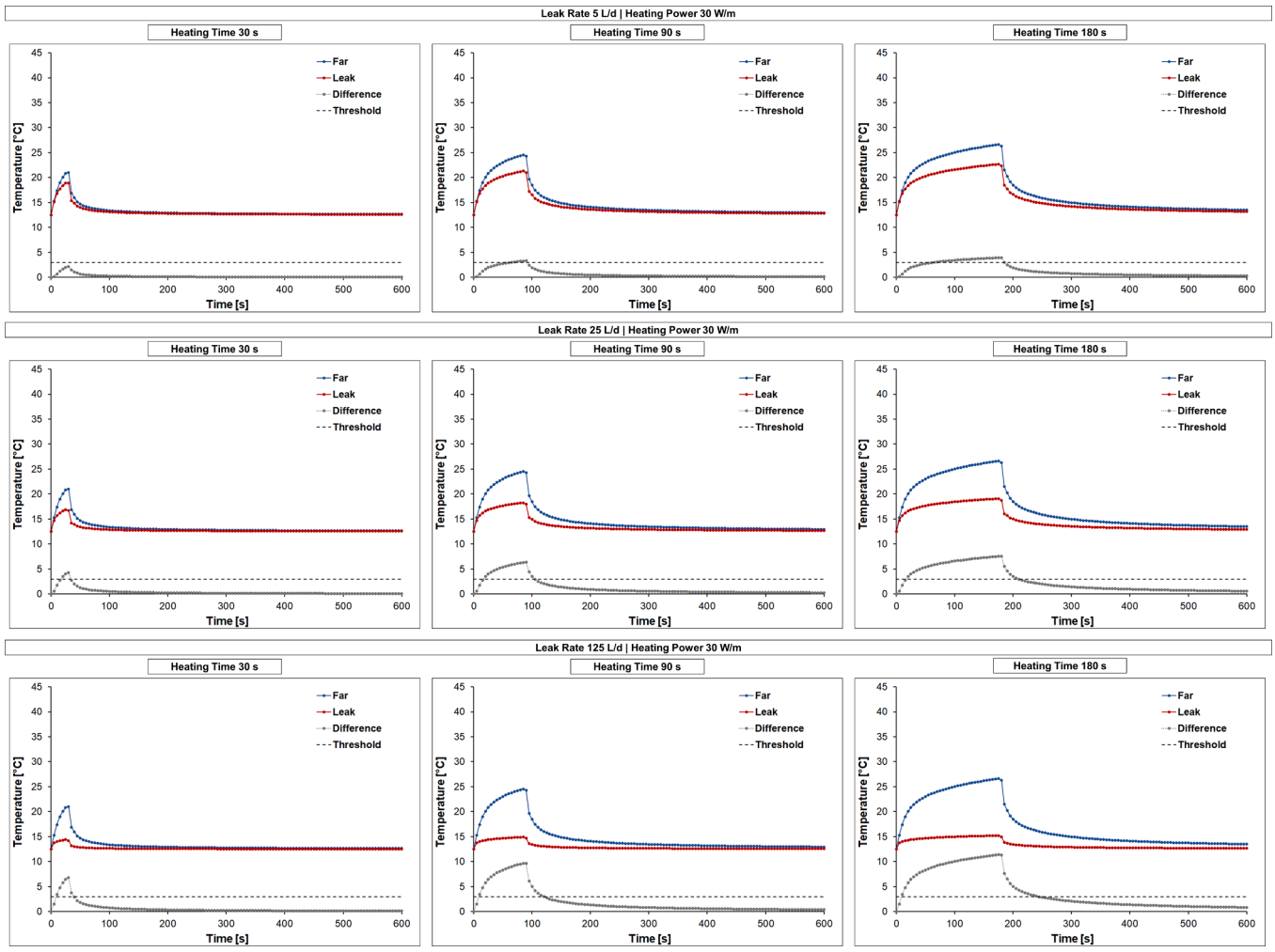

Fig. 7. Predicted temperature recorded over time along the actively heated fiber optic sensor at the farthest point from the leak ("Far") and at the leaky joint ("Leak") together with the difference over time ("Difference") between the predicted temperatures at these locations for all scenarios with heating power of 30 W/m. The dashed line represents the chosen detection threshold of 3 °C.

the power supply required for active heating, on the presence of other heat sources/sinks within the subsurface, and on soil/water temperature fluctuations.

The convective nature of the heat transfer mechanisms occurring around the active sensor once reached by leaked water (sec. 3.) could also make leak quantification possible. Indeed, the maximum difference between temperatures recorded along the active sensor at the farthest point from the leak ("Far") and at the leaky joint ("Leak") at the end of the heating phase if plotted versus the leak rate (Fig. 10) shows a clear nonlinear relationship that could be used to quantify leaks. Consistently with sec. 3., at given heating power and time, the maximum temperature difference recorded increases with increasing leak rate, eventually leading towards a plateau once a certain value of the leak rate is reached, whereas, at given leak rate, this temperature difference increases more with increasing heating power and less with increasing heating time. Therefore, simple expressions linking the leak rate to the maximum temperature difference recorded could be established in practical applications if a series of ADTS recordings were available and with a proper calibration of a model (either numerical or experimental) representative of on-site conditions. In addition, the length of active sensor affected by the temperature drop could also be used to help quantify leaks, although differences in this regard were far less pronounced in the modeled scenarios as the leak rate varied (Fig. 5).

It is also worth noting that heating powers and times modeled in this study produce a modest temperature rise (up to a maximum temperature at the actively heated sensing cable ranging between 15.3 and 40.6 °C) that is very limited in time and space (of just few minutes and up to 1–2 cm around the active sensor) and is not sufficient to induce any appreciable change to the flow field within the surrounding subsurface. This is indeed reassuring for practical applications since there would be a reduced possibility of i) altering water temperature and quality within the nearby pipe, ii) of inducing the mobilization of contaminants within the subsurface (which presence is not unlikely in urban environments), iii) of modifying leaked water pathways, iv) and of altering soil/groundwater temperature and properties.

Overall, the numerical evidence provided within this study is promising, especially because these results were obtained in absence of any temperature difference between water flowing within the pipe and the surrounding subsurface, and by placing the actively heated fiber optic sensor at distance from the pipe, on one of its sides (Fig. 1; sec. 2.1.), in a location suitable for both new and existing pipelines (particularly desirable for retrofit interventions), as well as for passive sensors, thus providing considerable flexibility in operation. Indeed, the same fiber optic cable used as active sensor could then be used as passive sensor once a suitable temperature difference between water inside the pipe and the surrounding subsurface is established on site, thus temporarily removing the cost of the power supply required for active heating.

However, the analysis described here is by no means conclusive, as it is intended as a preliminary investigation to support future field scale

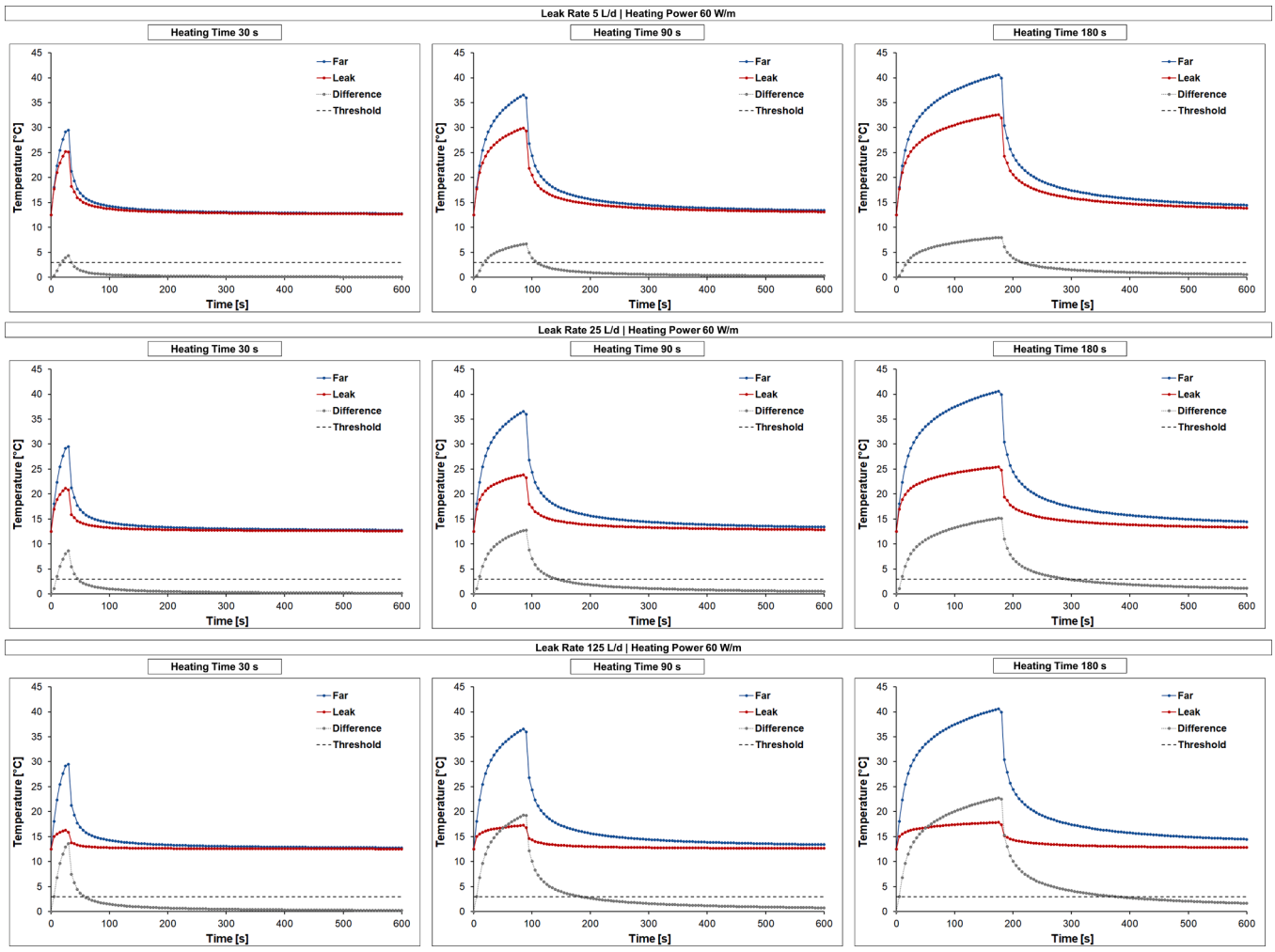

Fig. 8. Predicted temperature recorded over time along the actively heated fiber optic sensor at the farthest point from the leak ("Far") and at the leaky joint ("Leak") together with the difference over time ("Difference") between the predicted temperatures at these locations for all scenarios with heating power of 60 W/m. The dashed line represents the chosen detection threshold of 3 °C.

experiments and applications of active fiber optic distributed temperature sensing. Indeed, additional experimental evidence is required to validate these preliminary findings, in order to establish on the field the actual operational limits of this technology with regards to background leakages and its suitability for detecting, locating, and quantifying leaks in water infrastructure.

5. Conclusions

This study addressed for the first time the use of active distributed temperature sensing (ADTS) to detect background leakages in water infrastructure, offering a detailed transient analysis of the thermal response around an actively heated fiber optic sensor to a wide range of background leakages (5, 25, and 125 L/d) in a realistic 3D numerical environment, accounting for the effects of different heating powers (10, 30, and 60 W/m) and times (30, 90, and 180 s), of the unsaturated zone, and of fluid properties variation with temperature. Despite the absence of an initial temperature difference between leaked water and the surrounding soil, the analysis shows that there is potential to detect and locate incredibly small leaks in buried water pipelines with ADTS. Indeed, actively heating a fiber optic sensing cable at 30 W/m for 90 s could be sufficient to overcome a detection threshold of 3 °C for leaks as small as 5 L/d, whereas a heating power of 10 W/m for 90 s proved to be sufficient for leaks as low as 125 L/d. Instead, increasing the heating power up to 60 W/m allowed to overcome this detection threshold for the smallest leak modeled (5 L/d) with the shortest heating time (30 s). However, the analysis also shows that it is crucial to determine for how long the detection threshold is overcome, and that choosing the highest heating power possible is not necessarily the answer for a successful leak detection strategy with ADTS. Indeed, a compromise should be found between heating power and time depending on the acquisition time of the DTS system, on the monitoring strategy, on the cost of the power supply required for active heating, on the presence of other heat sources/sinks within the subsurface, and on soil/water temperature fluctuations.

As expected, in the modeled scenarios predicted temperature alterations show that forced convection is the main heat transfer mechanism around the active sensor once reached by leaked water and that the maximum recorded temperature difference between leak and non-leak locations occurs at the end of the heating phase. Clear nonlinear relationships between this temperature difference and the leak rate were predicted, information that could be used in practical applications to quantify background leakages, given that a series of ADTS recordings were available and with proper calibration of a model (either numerical or experimental) representative of on-site conditions.

It is also worth noting that these results were obtained by placing the actively heated fiber optic sensor in a location suitable for both new and existing pipelines, which is particularly desirable for retrofit interventions, and for non-heated fiber optic sensors (passive sensors), which would allow to use the same sensor either in active or in passive

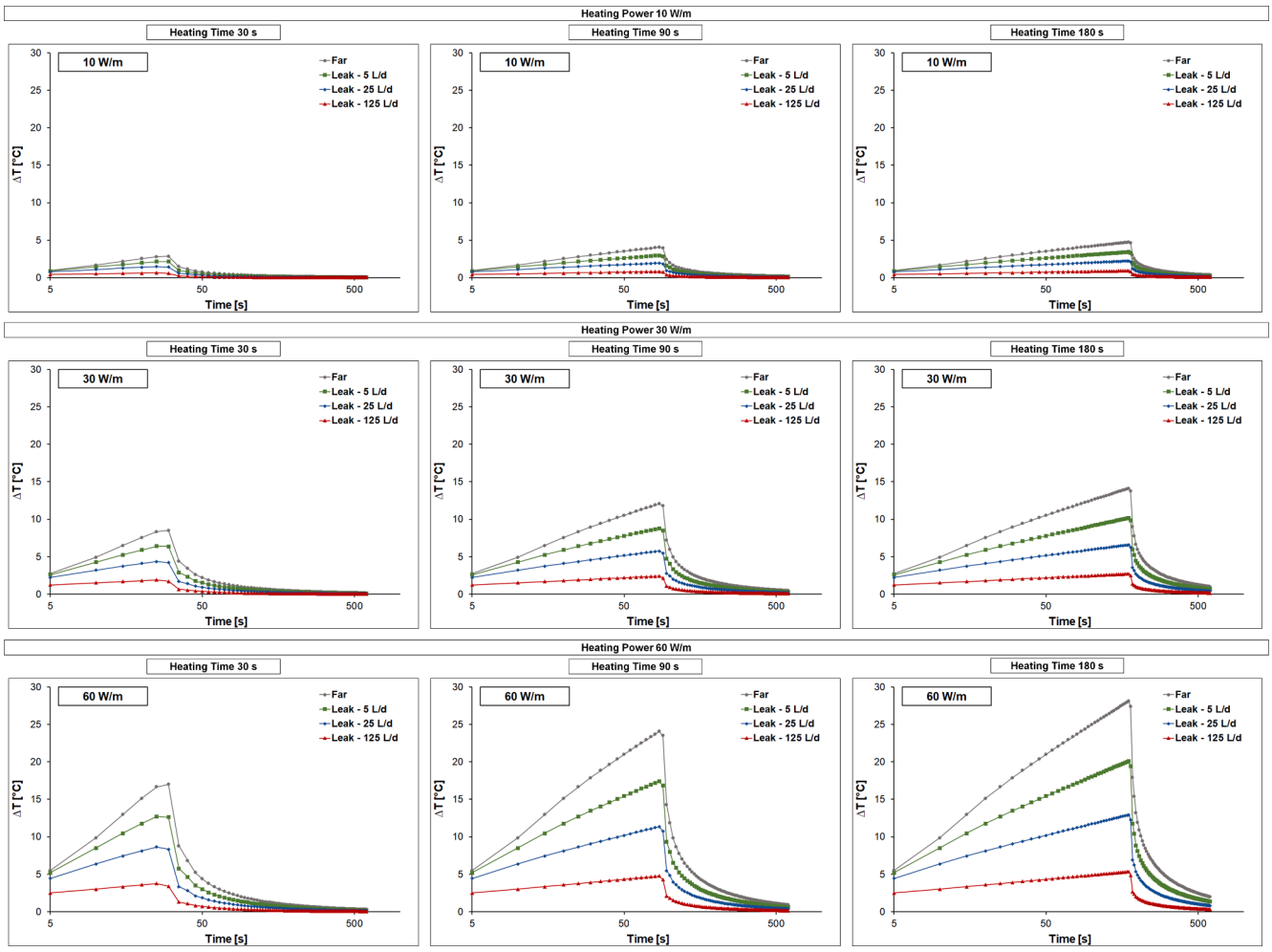

Fig. 9. Predicted temperature variations over time with respect to the temperature prior to active heating (ΔT) recorded along the actively heated fiber optic sensor at the farthest point from the leak ("Far") and at the leaky joint ("Leak") plotted on a semi-$\log_{10}$ scale for all scenarios.

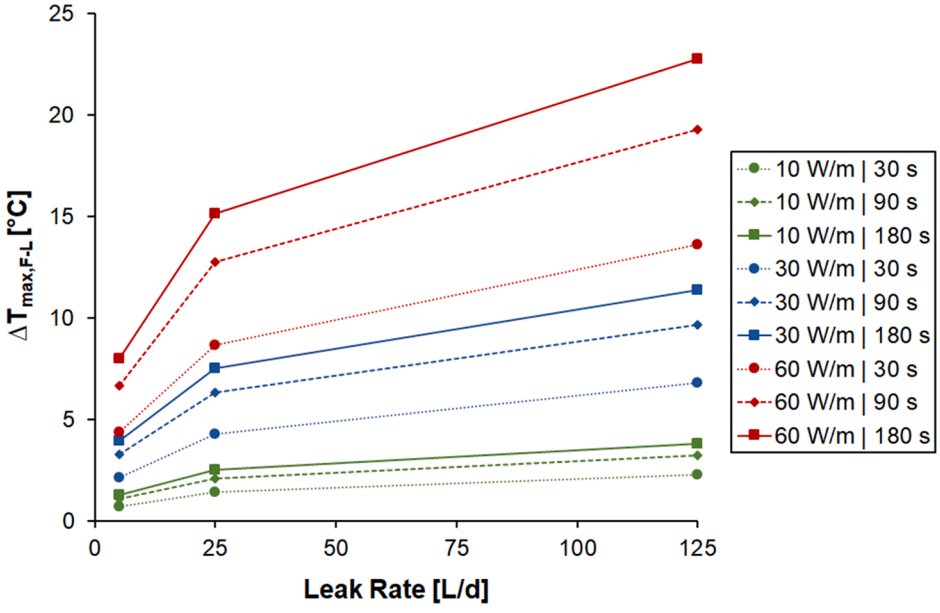

Fig. 10. Predicted maximum difference between temperatures recorded along the actively heated fiber optic sensor at the farthest point from the leak ("Far") and at the leaky joint ("Leak") at the end of the heating phase ($\Delta T_{max,F\text{-}L}$) plotted versus the leak rate for all scenarios.

mode depending on the temperature difference between water inside the pipeline and the surrounding subsurface, thus providing more flexibility in operation and an opportunity to temporarily remove the cost of the power supply required for active heating. Furthermore, for practical applications it is also reassuring that heating powers and times modeled in this study produced only a modest temperature rise (up to a maximum of 40.6 °C), very limited in time and space (of just few minutes and up to 1–2 cm around the active sensor), which was not sufficient to induce any significant change to the flow field within the surrounding subsurface. This suggests that the chance of altering temperature and quality of both water flowing within the nearby pipe and surrounding soil/groundwater would be very limited.

At this stage, the new theoretical and practical insights gained with this research support the feasibility of using ADTS to monitor the health of kilometers long water infrastructure and, specifically, to detect, locate, and quantify background leakages with a detection threshold that would require reasonable temperature and spatial resolutions. This type of leakages would remain undetected otherwise, thus hindering a proper formulation of pressure management strategies as well as maintenance, repair, and rehabilitation operations that would prevent further deterioration of the water infrastructure and reduce the large amount of water lost through these small but persistent and ubiquitous leaks. However, further experimental evidence is needed to validate the preliminary findings presented in this study, in order to establish on the field the actual capabilities of this promising technology.

Funding

The authors declare that no funds, grants, or other support were received during the preparation of this manuscript.

CRediT authorship contribution statement

Andrea D'Aniello: Writing – review & editing, Writing – original draft, Visualization, Validation, Methodology, Investigation, Formal analysis, Conceptualization. **Luigi Cimorelli:** Writing – review & editing, Validation. **Domenico Pianese:** Writing – review & editing, Validation.

Declaration of competing interest

The authors declare that they have no known competing financial interests or personal relationships that could have appeared to influence the work reported in this paper.

Data availability

All data supporting this study are available within the manuscript.

Appendix

Governing equations: unsaturated flow in porous media

The Richards' Equation interface (Subsurface Flow module) of COMSOL Multiphysics® version 6.1.0.346 solves the pressure-based formulation of Richards' equation by the finite element method (Bear, 1972; Istok, 1989; COMSOL, 2022). In order to account for fluid properties variation with temperature without resorting to the Oberbeck-Boussinesq approximation (Nield and Bejan, 2013), the generalized form of the equation of transient groundwater flow through variably water saturated porous media (Bear, 1972; Istok, 1989) was employed:

$$\frac{\partial \rho_w \theta_w}{\partial t} - \nabla \bullet \left[\frac{\rho_w k k_{rw}}{\mu_w} \left(\nabla p_w - \rho_w \underline{g} \right) \right] = Q_w \tag{1}$$

with $\theta_w = S_w \phi$ the soil water content, S_w the water saturation, ϕ the porosity, p_w the water pressure, k the intrinsic permeability (a scalar or a tensor depending on the presence of anisotropy), k_{rw} the relative permeability, ρ_w the water density, μ_w the water dynamic viscosity, $\underline{g}$ the gravity vector, and Q_w the water mass rate per unit volume (source/sink term). Water saturation S_w is expressed as a function of the effective water saturation $\overline{S}_w = \frac{S_w - S_{w,r}}{1 - S_{w,r}}$, which varies between 0 and 1. If the soil is fully water saturated ($S_w = 1$), water content equals porosity and is referred to as saturated water content θ_s, whereas if the soil is at its residual water saturation ($S_w = S_{w,r}$), it is referred to as residual water content θ_r.

The soil capillary pressure–saturation constitutive relationship is defined according to the van Genuchten retention curve (van Genuchten, 1980):

$$\overline{S}_w = \left[\frac{1}{1 + (\alpha h_{aw})^n} \right]^m \tag{2}$$

with h_{aw} the capillary pressure head between air (subscript a) and water (subscript w), namely $h_{aw} = h_a - h_w = -h_w = -\frac{p_w}{\rho_w g}$ (as $h_a = 0$ under the basic assumptions of groundwater flow through variably water saturated porous media) being h the pressure head and g the gravitational constant, α and n the van Genuchten parameters, and $m = 1 - 1/n$ with $n > 1$ according to Mualem's model (Mualem, 1976).

Relative permeability is related to the hydraulic conductivity $K_w = k_{rw} K_{sw}$, with $K_{sw} = \frac{\rho_w g}{\mu_w} k$ the saturated hydraulic conductivity, and is expressed with the van Genuchten-Mualem function (Mualem, 1976; van Genuchten, 1980):

$$k_{rw} = \overline{S}_w^{\,1/2} \left[1 - \left(1 - \overline{S}_w^{\,1/m} \right)^m \right]^2 \tag{3}$$

which varies from 0 ($\overline{S}_w = 0$) to 1 ($\overline{S}_w = 1$).

Governing equations: heat transfer in porous media

Under the assumption of local thermal equilibrium, the Heat Transfer in Porous Media interface (Heat Transfer module) of COMSOL Multiphysics® version 6.1.0.346 solves the following form of the heat equation by the finite element method (Nield and Bejan, 2013; COMSOL, 2022):

$$(\rho c)_e \frac{\partial T}{\partial t} + \rho_w c_{p,w} \underline{u} \bullet \nabla T - \nabla \bullet (k_e \nabla T) = Q \tag{4}$$

with $(\rho c)_e$ the effective heat capacity per unit volume, T the temperature, ρ_w the water density, $c_{p,w}$ the water specific heat at constant pressure, $\underline{u}$ the apparent groundwater velocity field, k_e the effective thermal conductivity (a scalar or a tensor depending on the presence of anisotropy), and Q the heat rate per unit volume (source/sink term).

For a variably water saturated porous medium, the effective heat capacity per unit volume becomes:

$$(\rho c)_e = (1-\phi)\rho_s c_s + \theta_w \rho_w c_{p,w} + \theta_a \rho_a c_{p,a} \tag{5}$$

whereas the effective thermal conductivity, assuming heat conduction occurring in parallel in the solid and fluid phases:

$$k_e = (1-\phi)k_s + \theta_w k_w + \theta_a k_a \tag{6}$$

with ϕ the porosity, ρ_s the solid phase density, c_s the solid phase specific heat, θ_w the soil water content, θ_a the soil air content, ρ_a the air density, $c_{p,a}$ the air specific heat at constant pressure, k_s the solid phase thermal conductivity, k_w the water thermal conductivity, and k_a the air thermal conductivity. In presence of thermal dispersion, the term $k_d = \rho_w c_{p,w} D_{ij}$ is added to the right-hand side of (6), with $D_{ij} = \lambda_{ijkl} \frac{v_k v_l}{|\underline{v}|}$ the dispersion tensor, λ_{ijkl} the dispersivity tensor (Nield and Bejan, 2013; COMSOL, 2022), $\underline{v} = \underline{u}/\theta_w$ and v_k, v_l the pore water velocity field and its components.

References

Adedeji, K.B., Hamam, Y., Abe, B.T., Abu-Mahfouz, A.M., 2017. Towards achieving a reliable leakage detection and localization algorithm for application in water piping networks: an overview. IEEE Access 5, 20272–20285.

Bear, J., 1972. Dynamics of fluids in porous media. Dover Publications Inc, New York.

Bolognini, G., Hartog, A., 2013. Raman-based fibre sensors: Trends and applications. Opt. Fiber Technol. 19 (6), 678–688.

Carsel, R.F., Parrish, R.S., 1988. Developing joint probability distributions of soil water retention characteristics. Water Resour. Res. 24 (5), 755–769.

McKinsey & Company (2009) The global corporate water footprint. Risks, opportunities, and management options. CCSI Water & Adaptation Service Line. https://www.mckinsey.com/~/media/mckinsey/dotcom/client_service/sustainability/pdfs/report_large_water_users.aspx. Accessed 15 June 2023.

COMSOL (2022) Subsurface Flow Module User's Guide – Version 6.1. COMSOL Multiphysics. https://doc.comsol.com. Accessed 26 June 2023.

D'Aniello, A., 2023. Detecting background leakages in water infrastructure with fiber optic distributed temperature sensing: insights from a heat transfer-unsaturated flow model. Water Resour. Manag. 37 (14), 5535–5558. https://doi.org/10.1007/s11269-023-03617-7.

Dalla Santa, G., Galgaro, A., Sassi, R., Cultrera, M., Scotton, P., Mueller, J., Bernardi, A., 2020. An updated ground thermal properties database for GSHP applications. Geothermics 85, 101758.

D'Aniello, A., Cimorelli, L., Pianese, D., 2021. Leaking pipes and the urban karst: a pipe scale numerical investigation on water leaks flow paths in the subsurface. J. Hydrol. 603, 126847 https://doi.org/10.1016/j.jhydrol.2021.126847.

D'Aniello, A., Cimorelli, L., Pianese, D., 2022. Utility trenches: sinks or barriers? Modeling the fate of leaked water in a crowded subsurface. J. Hydrol. 612, 128303 https://doi.org/10.1016/j.jhydrol.2022.128303.

del Val, L., Carrera, J., Pool, M., Martínez, L., Casanovas, C., Bour, O., Folch, A., 2021. Heat dissipation test with fiber-optic distributed temperature sensing to estimate groundwater flux. Water Resour. Res. 57(3):e2020WR027228.

Diersch, H.J.G., 2014. FEFLOW: finite element modeling of flow, mass and heat transport in porous and fractured media. Springer-Verlag, Berlin Heidelberg.

Drusová, S., Bakx, W., Doornenbal, P.J., Wagterveld, R.M., Bense, V.F., Offerhaus, H.L., 2021. Comparison of three types of fiber optic sensors for temperature monitoring in a groundwater flow simulator. Sens Actuator A Phys 331, 112682.

FAO – Food and Agriculture Organization of the United Nations (2012) Coping with water scarcity – An action framework for agriculture and food security. FAO Water Reports 38, Rome.

A.K. Howard Pipe Bedding and Backfill Geotechnical Training Manual No. 7, United States Department of the Interior, Bureau of Reclamation, Technical Service Center, Geotechnical Services 1996 Denver, Colorado.

Hu, Z., Chen, B., Chen, W., Tan, D., Shen, D., 2021. Review of model-based and data-driven approaches for leak detection and location in water distribution systems. Water Supply 21 (7), 3282–3306.

Ibrahim, K., Tariq, S., Bakhtawar, B., Zayed, T., 2021. Application of fiber optics in water distribution networks for leak detection and localization: a mixed methodology-based review. H2Open J 4 (1), 244–261.

Inaudi, D., Belli, R., Walder, R., 2008. Detection and localization of micro-leakages using distributed fiber optic sensing. International Pipeline Conference 48579, 599–605.

IPCC – Intergovernmental Panel on Climate Change (2023) IPCC, 2023: Summary for Policymakers. In: Climate Change 2023: Synthesis Report. A Report of the Intergovernmental Panel on Climate Change. Contribution of Working Groups I, II and III to the Sixth Assessment Report of the Intergovernmental Panel on Climate Change [Core Writing Team, H. Lee and J. Romero (eds.)]. IPCC, Geneva, Switzerland, 36 pages. https://www.ipcc.ch/report/ar6/syr/. Accessed 15 June 2023.

Istok JD (1989) Groundwater modelling by the finite element method. Water Resources Monograph, 13, American Geophysical Union Florida Avenue 2000 NW Washington, DC 2000.

Lambert AO (2009) Ten years experience in using the UARL formula to calculate infrastructure leakage index. International Water Association (IWA) Waterloss Conference 2009 Cape Town South Africa.

A.O. Lambert R. McKenzie Practical experience in using the Infrastructure Leakage Index International Water Association (IWA) Conference "leakage Management: A Practical Approach" 2002 Lemesos, Cyprus.

Lambert, A.O., Brown, T.G., Takizawa, M., Weimer, D., 1999. A review of performance indicators for real losses from water supply systems. J Water SRT –. Aqua 48 (6), 227–237.

Lambert, A., Trow, S., Merks, C., Charalambous, B., Donnelly, A., Galea St John, S., Fantozzi, M., Hulsmann, A., Koelbl, J., Kovač, J., Schipper, D., 2015a. EU reference document good practices on leakage management WFD CIS WG PoM – main report. Office Official Publ. Eur. Communities, Luxembourg, European Union.

Lambert, A., Trow, S., Merks, C., Charalambous, B., Donnelly, A., Galea St John, S., Fantozzi, M., Hulsmann, A., Koelbl, J., Kovač, J., Schipper, D., 2015b. EU Reference Document Good Practices on Leakage Management WFD CIS WG PoM – Case Study document. Office for Official Publications of the European Communities, Luxembourg, European Union.

Li, R., Huang, H., Xin, K., Tao, T., 2015. A review of methods for burst/leakage detection and location in water distribution systems. Water Sci. Technol. Water Supply 15 (3), 429–441.

Li, W., Liu, T., Xiang, H., 2021. Leakage detection of water pipelines based on active thermometry and FBG based quasi-distributed fiber optic temperature sensing. J. Intell. Mater. Syst. Struct. 32 (15), 1744–1755.

Li, H.J., Zhu, H.H., Tan, D.Y., Shi, B., Yin, J.H., 2023. Detecting pipeline leakage using active distributed temperature Sensing: Theoretical modeling and experimental verification. Tunn. Undergr. Space Technol. 135, 105065.

Liemberger, R., Wyatt, A., 2019. Quantifying the global non-revenue water problem. Water Supply 19 (3), 831–837.

Liu, X.F., Zhu, H.H., Wu, B., Li, J., Liu, T.X., Shi, B., 2023. Artificial intelligence-based fiber optic sensing for soil moisture measurement with different cover conditions. Measurement 206, 112312.

Lombera RR, Serrano JM, Martinez O, San Emeterio JD, Lopez-Higuera JM (2014) Experimental demonstration of a leakage monitoring system for large diameter water pipes using a fiber optic distributed sensor system. In SENSORS, 2014 IEEE Conference, pp. 1885-1888.

M. Mazzucato N. Okonjo-Iweala J. Rockström T. Shanmugaratnam Turning the Tide: A Call to Collective Action Global Commission on the Economics of Water (GCEW) 2023 Paris.

Milano, V., 2012. Acquedotti – Guida alla progettazione. Hoepli Editore, Milano.

Motil, A., Bergman, A., Tur, M., 2016. State of the art of Brillouin fiber-optic distributed sensing. Opt. Laser Technol. 78, 81–103.

Mualem, Y., 1976. A new model for predicting the hydraulic conductivity of unsaturated porous media. Water Resour. Res. 12 (3), 513–522.

Nield, D.A., Bejan, A., 2013. Convection in Porous Media. Springer Science+Business Media, New York.

Niklès, M., Vogel, B.H., Briffod, F., Grosswig, S., Sauser, F., Luebbecke, S., Pfeiffer, T., 2004. Leakage detection using fiber optics distributed temperature monitoring. In Smart Structures and Materials 2004: Smart Sensor Technology and Measurement Systems. Proc. SPIE 5384, 18–25.

Simon, N., Bour, O., Lavenant, N., Porel, G., Nauleau, B., Klepikova, M., 2023. Monitoring groundwater fluxes variations through active-DTS measurements. J. Hydrol. 129755.

Stokes, C.S., Simpson, A.R., Maier, H.R., 2014. The cost–greenhouse gas emission nexus for water distribution systems including the consideration of energy generating

infrastructure: an integrated conceptual optimization framework and review of literature. Earth Perspectives 1 (1), 1–17.
Su, H., Tian, S., Kang, Y., Xie, W., Chen, J., 2017. Monitoring water seepage velocity in dikes using distributed optical fiber temperature sensors. Autom. Constr. 76, 71–84.
Sun, M.Y., Shi, B., Zhang, D., Liu, J., Guo, J.Y., Wei, G.Q., Cheng, W., 2020. Study on calibration model of soil water content based on actively heated fiber-optic FBG method in the in-situ test. Measurement 165, 108176.
Sun, M.Y., Shi, B., Cui, Y.J., Tang, C.S., Zheng, X., Zhong, P., Tong, Y.P., 2022. Evaluating three measurement methods of soil ground heat flux based on actively heated distributed temperature sensing technology. Eng. Geol. 303, 106649.
The Engineering ToolBox, 2001. Free tools and information for engineering and design of technical applications. Accessed 26 June 2023. https://www.engineeringtoolbox.com/.
United States Department of Agriculture Soil Conservation Service – USDA SCS, 1987. Soil Mechanics Level 1, Module 3 – USDA Soil Textural Classification. Study Guide, USDA Soil Conservation Service, Washington DC.
van Genuchten, M.T., 1980. A closed-form equation for predicting the hydraulic conductivity of unsaturated soils. Soil Sci. Soc. Am. J. 44 (5), 892–898.
Vidana Gamage, D.N., Biswas, A., Strachan, I.B., 2018. Actively heated fiber optics method to monitor three-dimensional wetting patterns under drip irrigation. Agric Water Manag 210, 243–251.
Waltham, T., Bell, F.G., Culshaw, M.G., 2005. Sinkholes induced by engineering works. Sinkholes and Subsidence: Karst and Cavernous Rocks in Engineering and Construction. Springer, Berlin, Heidelberg.
Wang, Q., Gu, X., Zhang, Z., Long, Z., Zhao, Y., 2022. On-line leakage detection in buried tap water distribution pipes using distributed temperature sensing. J. Pipeline Syst. Eng. Pract. 13 (2), 04022010.
Wang, L., Narasimman, S.C., Ravula, S.R., Ukil, A., 2017. Water ingress detection in low-pressure gas pipelines using distributed temperature sensing system. IEEE Sens. J. 17 (10), 3165–3173.
Water, Y., 2018. Mains Design and Construction Guidelines for Self-Lay Providers. Accessed 20 June 2023. https://www.yorkshirewater.com/.
Wijaya, H., Rajeev, P., Gad, E., 2021. Distributed optical fibre sensor for infrastructure monitoring: Field applications. Opt. Fiber Technol. 64, 102577.
Xu, Y., Li, J., Zhang, M., Yu, T., Yan, B., Zhou, X., Gao, S., 2020. Pipeline leak detection using Raman distributed fiber sensor with dynamic threshold identification method. IEEE Sens. J. 20 (14), 7870–7877.
Zhang B, Gu K, Bayer P, Qi H, Shi B, Wang B, ... Zhou Q (2023) Estimation of Groundwater Flow Rate by an Actively Heated Fiber Optics Based Thermal Response Test in a Grouted Borehole. Water Resour Res e2022WR032672.
Zhu, H.H., Wang, J.C., Reddy, N.G., Garg, A., Cao, D.F., Liu, X.F., Shi, B., 2022. Monitoring infiltration of capillary barrier with actively heated fibre Bragg gratings. Environ Geotech 40, 1–16.
S. Ziemendorff Comparison of suitable leak detection methods. Selection Guideline with special consideration of the conditions in countries with emerging markets and developing economies Deutsche Gesellschaft Für Internationale Zusammenarbeit (GIZ) GmbH 1st Edition, 2022 Eschborn 10.5281/zenodo.6625858.